Front. Earth Sci. 2017, 11(1): 184–201
DOI 10.1007/s11707-016-0565-4

RESEARCH ARTICLE

Shale gas reservoir characteristics of Ordovician-Silurian formations in the central Yangtze area, China

Chang'an SHAN[1,2], Tingshan ZHANG (✉)[2,3], Yong WEI[4], Zhao ZHANG[5]

1 School of Earth Sciences and Engineering, Xi'an Shiyou University, Xi'an 710065, China
2 State Key Laboratory of Oil and Gas Reservoir Geology and Exploration, Southwest Petroleum University, Chengdu 610500, China
3 School of Geoscience and Technology, Southwest Petroleum University, Chengdu 610500, China
4 Exploration and Development Research Institute, Southwest Oil & Gas field Company, CNPC, Chengdu 610041, China
5 Exploration and Development department, Zhejiang Oilfield Company, CNPC, Hangzhou 310023, China

Abstract The characteristics of a shale gas reservoir and the potential of a shale gas resource of Ordovician–Silurian age in the north of the central Yangtze area were determined. Core samples from three wells in the study area were subjected to thin-section examination, scanning electron microscopy, nuclear magnetic resonance testing, X-ray diffraction mineral analysis, total organic carbon (TOC) testing, maturity testing, gas-bearing analysis, and gas component and isothermal adsorption experiments. A favorable segment of the gas shale reservoir was found in both the Wufeng Formation and the lower part of the Longmaxi Formation; these formations were formed from the late Katian to early Rhuddanian. The high-quality shale layers in wells J1, J2, and J3 featured thicknesses of 54.88 m, 48.49 m, and 52.00 m, respectively, and mainly comprised carbonaceous and siliceous shales. Clay and brittle minerals showed average contents of 37.5% and 62.5% (48.9% quartz), respectively. The shale exhibited type II_1 kerogens with a vitrinite reflectance ranging from 1.94% to 3.51%. TOC contents of 0.22%–6.05% (average, 2.39%) were also observed. The reservoir spaces mainly included micropores and microfractures and were characterized by low porosity and permeability. Well J3 showed generally high gas contents, i.e., 1.12–3.16 m^3/t (average 2.15 m^3/t), and its gas was primarily methane. The relatively thick black shale reservoir featured high TOC content, high organic material maturity, high brittle mineral content, high gas content, low porosity, and low permeability. Shale gas adsorption was positively correlated with TOC content and organic maturity, weakly positive correlated with quartz content, and weakly negatively correlated with clay content. Therefore, the Wufeng and Longmaxi formations in the north of the central Yangtze area have a good potential for shale gas exploration.

Keywords reservoir characteristic, shale gas, Upper Ordovician, Lower Silurian, central Yangtze area

1 Introduction

The success of commercial shale gas development in the US has attracted worldwide attention and led to renewed interest in argillaceous rocks in recent years (Montgomery et al., 2005; Loucks et al., 2009). A detailed understanding of the characteristics of gas shale reservoirs can help in the accurate evaluation of potential shale gas resources.

The Lower Cambrian (Qiongzhusi and Niutitang formations) and Upper Ordovician to Lower Silurian (Wufeng and Longmaxi formations) marine shales, located south of the Sichuan Basin in the upper Yangtze area, China are considered the shale gas strata with the most potential for exploration (Xiao et al., 2012). Several national demonstration areas for marine shale gas exploration and production have been established. Black shale from the Upper Ordovician Wufeng Formation and the Lower Silurian Longmaxi Formation in the central Yangtze area has been widely developed (Li et al., 2011; Long, 2011; Qiu et al., 2013). The characteristics of the gas shale reservoir in the upper Yangtze area have been extensively investigated (Kang, 2012; Zhou et al., 2012; Teng and Liu, 2013, Guo and Zhang, 2014). However, similar studies on the Wufeng and Longmaxi formations in the central Yangtze area have received little attention until very recently (Qiu et al., 2013).

China National Petroleum Corporation (CNPC) has drilled two shallow and nearly entirely cored shale gas

Received December 6, 2014; accepted October 22, 2015

E-mail: zts_3@126.com

wells (J1 and J2), as well as a deep appraisal well (J3), in Yichang City, Hubei Province to determine the development of shale in the Wufeng and Longmaxi Formations (Fig. 1). The characteristics of the shale gas reservoir and the potential of the shale gas resource of Ordovician–Silurian age in the north of the central Yangtze area were determined in this work. Core samples from three wells were subjected to thin-section examination, scanning electron microscopy (SEM), nuclear magnetic resonance (NMR), X-ray diffraction (XRD) mineral analysis, total organic carbon (TOC) testing, maturity testing, gas-bearing analysis, and gas component and isothermal adsorption experiments. The present study characterized the shale gas reservoir in the aforementioned formations based on petrology, mineralogy, organic geochemistry, pore type, physical property, gas-bearing property, and adsorption capability of black shale.

2 Geologic setting

Continental crust of the middle Yangtze area formed in the Middle–Late Proterozoic on the foundation of the Archaeozoic–Early Proterozoic microland core after multiple stages of subsidence, folding, metamorphism, and consolidation (Liu et al., 2009). The geological structures mainly include synclinoria and anticlinoria. These structures can be divided into several secondary units, namely the Bahong thrust faulted anticline, the Huangling uplift, the Dangyang synclinorium, the Lexiangguan–Qianjiang anticlinorium, the Chenhu–Tuditang synclinorium, and the Chongyang–Tongshan thrust–anticline belt, according to the characteristics of the different formations (Fu et al., 2006) (Fig. 1).

The middle Yangtze area is covered by strata from the Proterozoic to the Cenozoic. The Pre-Sinian strata are mainly distributed along the Huangling uplift located east of Dangyang; some of the strata are also scattered in other areas. The Kongling, Dagushi, and Huashan groups form the ancient basement of the study area. The earliest sedimentary cover is Sinian. Palaeozoic strata (including the Upper Ordovician Wufeng Formation and Lower Silurian Longmaxi Formation) are distributed in the western, northern, and eastern areas. Mesozoic and Cenozoic strata are widely developed in the central area. The exposed formation from the Pre-Sinian metamorphic rock series to the Quaternary is approximately 20,000 m thick with over 7,800 m of sedimentary cover.

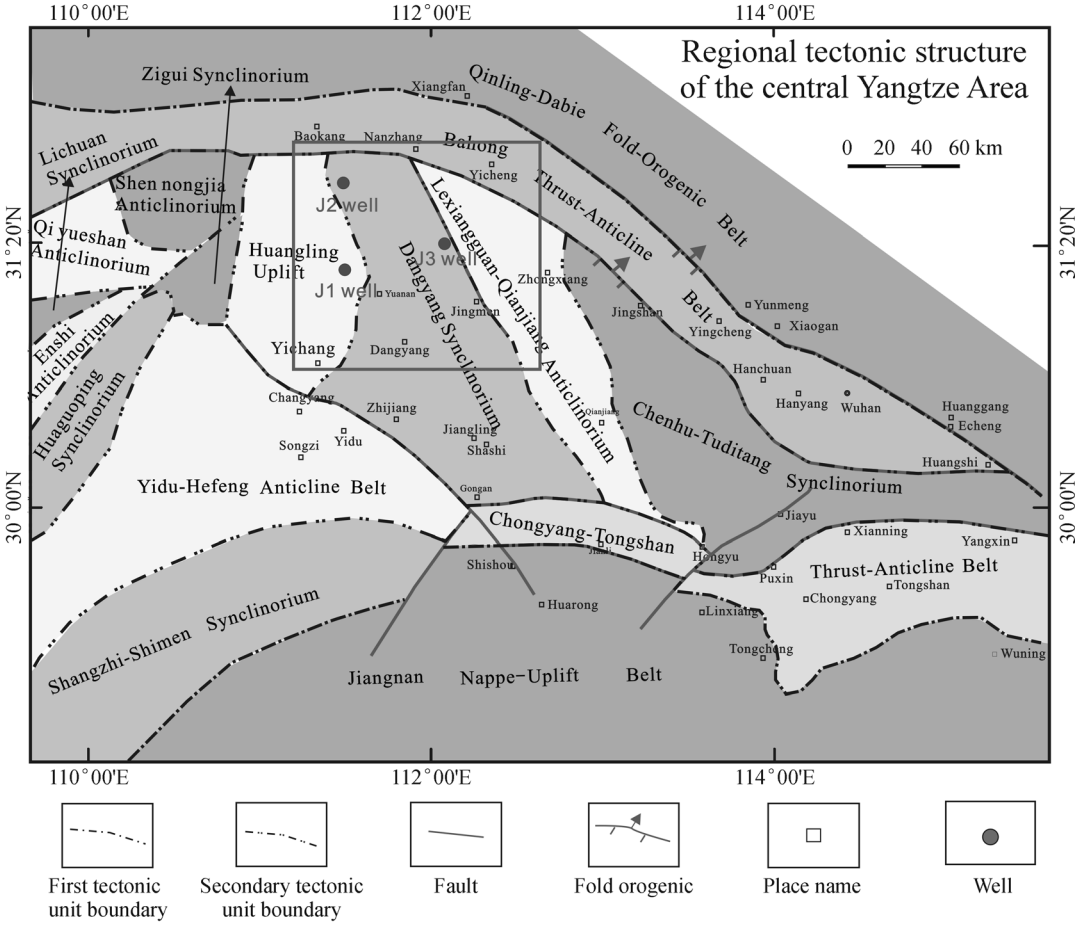

Fig. 1 Location of wells and regional tectonic structure of the middle Yangtze area: (a) location of the study area; (b) regional tectonic structure of middle Yangtze area (modified after Fu et al., 2006); (c) location of wells in the study area.

Land around the Yangtze block during the late Ordovician to the early Silurian continuously rose and caused most parts of the Yangtze area to become enclosed or semi-enclosed stagnant marine environments (Liu et al., 2009; Li et al., 2011; Mu et al., 2011). Black shale, which is common in the Wufeng and Longmaxi Formations in the middle and upper Yangtze areas, is rich in pyrite and graptolite fossils (Li and Wang, 2001; Wang et al., 2002). The rocks in these formations mainly comprise black shales, siliceous shales, and gray silty mudstones intercalated with thin layers of siltstone. These rocks also yield abundant and diverse graptolite faunas. The Kuanyinchiao Bed on top of the Wufeng Formation is characterized by argillaceous limestone and yields an abundant and diverse shelly fauna, i.e., the Hirnantia fauna (Chen et al, 2004).

3 Methods and samples

We combined core descriptions (i.e., consecutive core images) with thin-section examinations to characterize the petrology and mineralogy of core samples in accordance with the proposal of Papazis (2005). We used SEM to analyze the cores from the wells. A total of 30 samples from J1 in the Wufeng and Longmaxi formations were subjected to thin-section examination. Ten of these samples were examined via SEM. Another 21 shale samples from J1, J2, and J3 in the Wufeng Formation as well as the lower part of the Longmaxi Formation were examined via XRD. Thin sections were impregnated with both normal and fluorescent blue dyes, ground to 30 μm thickness, finished with a polished surface (0.5 mm diamond grit), and observed through UV light microscopy. Shale powder was analyzed by XRD using an X'Pert Pro X-ray diffractometer with a Cu anode at 40 kV, 20 mA, and 0.154 nm. Micropores and microfractures were observed under a Quanta TM450 scanning electron microscope under high vacuum.

Kerogen macerals of six samples from J3 were measured in accordance with the SY/T 5125-96 oil and gas industry standard of China to characterize the organic geochemistry of the black shale. This process was conducted under a biological microscope with transmission white light and fluorescence. A total of 48 samples (12 from J1 and 36 from J3) were treated with hydrochloric acid (1:1) to remove carbonate. Then, TOC contents of the samples were measured using an infrared LECO CS-400 carbon–sulfur analyzer. Shale organic matter maturity was evaluated in 20 (5 from J1 and 15 from J3) of the 48 samples. Black shale samples lacked vitrinite. Thus, pyrobitumen reflectance (BRr) of polished blocks was measured under reflected light using a microphotometric system. Percentage of random reflectance was measured in an oil immersion (n = 1.518) at 546 nm. BRr was converted into the equivalent vitrinite reflectance (VRr) by using the following equation (Schoenherr et al., 2007):

$$\mathrm{VRr} = (\mathrm{BRr} + 0.2443)/1.0495. \quad (1)$$

NMR was used to test the volume of movable fluid in pores and reflect the effective porosity of core samples. Porosity and bound water saturation were used to calculate the permeability of the core samples (Shang et al., 1998). In the present study, six core samples from the three wells were analyzed using a low-magnetic-field NMR core analyzer (RecCore04). All analyses were operated on the same plug to interrelate the analytical results.

Separated, residual, and lost gases were tested for shale gas content. In the present study, 4 black shale samples from J1 and 12 samples from J3 were collected to measure the shale gas content (following China National Standard GB/T 19559-2008) in the Key Laboratory of Unconventional Oil and Gas, CNPC. The compositions of 16 canisters of separated gas were analyzed using a gas analyzer (7890A) in accordance with China National Standard GB/T 13610-2003.

An isothermal adsorption device (ISO-200) was used to conduct isothermal adsorption tests on 10 core samples (4 from J1 and 6 from J3) based on the China National Standard GB/T 19560-2008 in the Key Laboratory of Unconventional Oil and Gas, CNPC. Adsorption of shale samples followed the Langmuir isothermal adsorption equation:

$$V = V_{\mathrm{L}} \times P/(P_{\mathrm{L}} + P), \quad (2)$$

where P is the gas pressure (MPa), V is the adsorption amount at pressure P ($\mathrm{cm^3/g}$), V_{L} is the Langmuir volume ($\mathrm{cm^3/g}$), and P_{L} is the Langmuir pressure (MPa).

The test data were highly consistent with the calculation results from the Langmuir equation.

4 Characteristics of the black shale reservoir

4.1 Strata thickness

Black shale layers in the Wufeng and Longmaxi Formations in J1, J2, and J3 are 302.35 m, 247.89 m, and 422.00 m thick, respectively. High-quality black shale developed in the Wufeng Formation as well as the lower part of the Longmaxi Formation. The high-quality black shale layers in J1, J2, and J3 are 54.88 m, 48.49 m, and 52.00 m thick, respectively (Fig. 2(a)). In J1 (Fig. 2(b)), the "63" layer (328.15–328.37 m) on top of the Wufeng Formation is a thin layer of bioclastic marlstone called the Kuanyinchiao Bed. The layers in the Wufeng Formation in J1 and J2 are 8.92 m and 8.00 m thick, respectively (Fig. 2 (a)). In addition, the Wufeng Formation in J3 may be inferred to be lacking because of a fault. This speculation is based on the absence of the Kuanyinchiao Bed in the shale core and the presence of a fault at the bottom of the Longmaxi Formation (Fig. 2(c)).

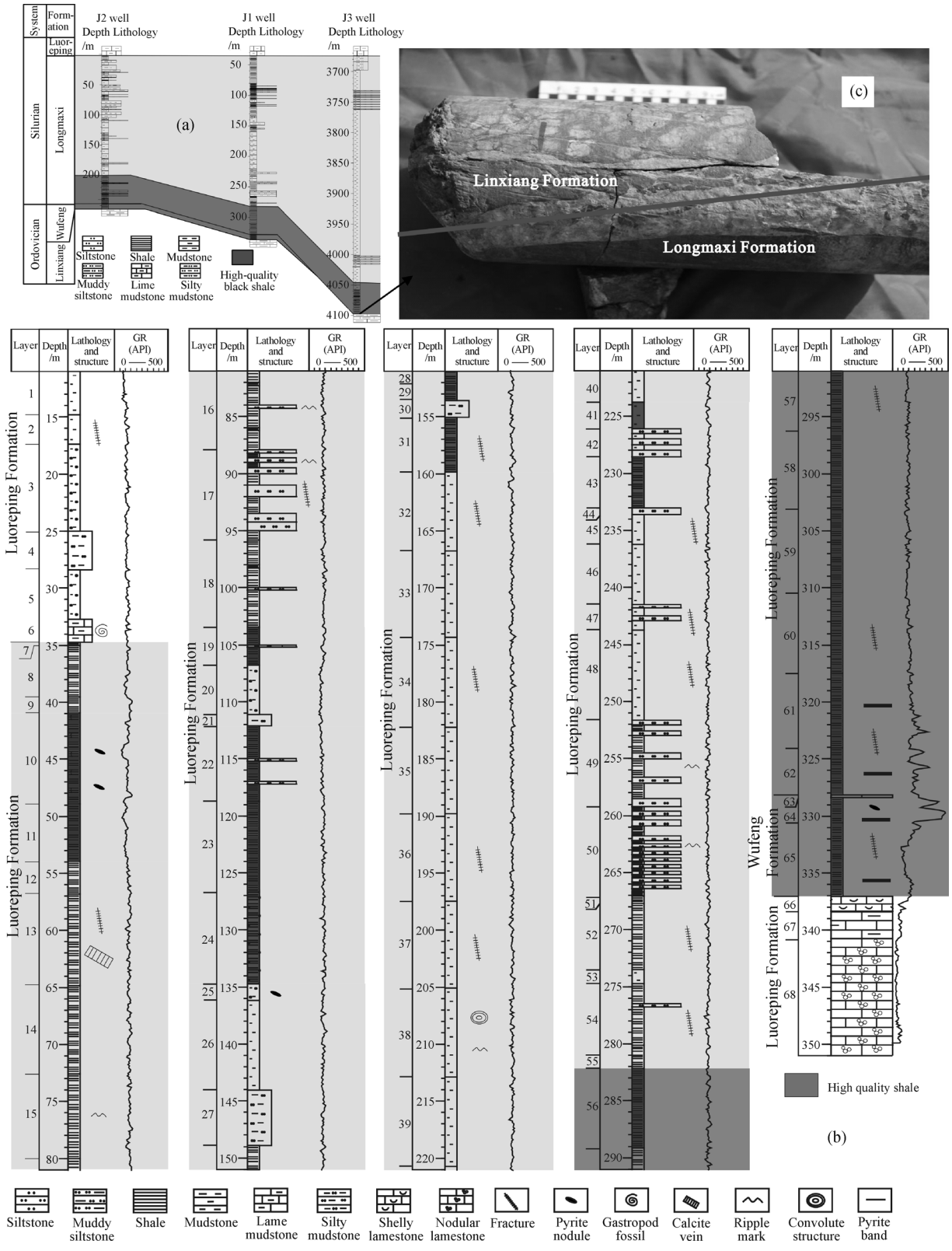

Fig. 2 (a) Cross section of three wells showing the stratigraphy in the Wufeng and Longmaxi Formations. (b) Lithologic characteristics of the cores in J1. (c) Core photo of J3, showing a fault at the bottom of Longmaxi Formation.

4.2 Lithofacies features

4.2.1 Mineral composition

A total of 21 shale samples show average contents of 37.5% clay (18%–53%), 48.9% quartz (37%–72%), 8.0% feldspar (2%–13%), 3.2% pyrite, and 2.4% carbonate rock (calcite and ankerite) (Table 1, Fig. 3(a)). Thus, the brittle minerals (the total average content of quartz, feldspar, pyrite, and carbonate) present an average content of 62.5%. The three wells are comparable with the shale gas wells in the southern Sichuan Basin. Rocks from the Changxin 1 well in the Longmaxi Formation show average contents of 40% clay (15%–75%), 34% quartz (30%–70%), 4.7% feldspar (1%–5%), and 18% carbonate rock (5%–30%). Rocks at the bottom (30 m) mainly comprise black lamellar lime shale and mudstone, which are rich in organic matter. Average clay and carbonate rock contents are 24.7% and 23.4%, respectively. Total average content of quartz, feldspar, and pyrite is 51.9% (44.2% quartz) (Chen et al., 2013). The main shale gas-producing layers in North America contain 28%–52% quartz (mainly biological and lithogenic quartz), 4%–16% carbonate rock, and 46%–60% brittle minerals (Liu et al., 2011) (Fig. 3(b)).

Clay minerals of the 21 shale samples in these wells show average relative contents of 48.3% illite (37%–58%), 22.6% chlorite (13%–31%), 16.9% mixed layers of illite and smectite (5%–28%), and 12.2% mixed layers of chlorite and smectite (0%–20%), in which the content of the former is low. Therefore, the clay minerals are mainly composed of illite. Clay mineral contents in these wells were comparable with those in shale gas wells (X1 and X2 wells) in the southern Sichuan Basin (Fig. 3(c)). The relative average content of non-expanded illite in the mixed layer of illite and smectite is 88% (85%–90%), whereas the content of chlorite in the mixed layer of chlorite and smectite is 61.3% (50%–77%) (Table 1). That implies unordered mixed-layer clay was replaced by ordered mixed-layer clay. Shale in the Wufeng and Longmaxi Formations apparently entered the late diagenesis phase (Ma et al., 2004).

4.2.2 Shale lithofacies

Four lithofacies can be identified in the Wufeng–Longmaxi shale based on the core and microscopic observations, according to the mineral composition. These lithofacies are

Table 1 Mineral content chart based on XRD analysis in the Wufeng–Longmaxi Formations in the J1, J2, and J3 wells

Well name	Depth/m	Formation	Lithology	Mineral composition/%							Clay composition/%				Mixer layer clays			
															I/S/%		C/S/%	
				Q	Pl	Ca	Py	Si	A	Cl	I	C	I/S	C/S	S	I	S	C
J1	292.6	Longmaxi (S_1l)	Black shale	44	11	0	2	0	0	43	53	24	6	17	15	85	41	59
	299.4			46	11	0	0	0	0	43	55	23	5	17	15	85	37	63
	310.8			46	10	0	3	0	0	41	57	23	5	15	10	90	50	50
	319.7			50	8	0	9	0	2	31	55	24	7	14	15	85	31	69
	327.2			66	8	0	3	0	2	21	52	31	17	0	10	90	0	0
	329.6	Wufeng (O_3w)	Black shale	71	4	0	2	0	4	19	48	21	13	18	10	90	31	69
	332.7			48	11	0	4	0	4	33	49	20	15	16	15	85	33	67
J2	200.0	Longmaxi (S_1l)	Black shale	45	10	0	0	0	0	45	43	30	15	12	15	85	41	59
	214.0			43	11	0	0	3	0	43	43	29	17	11	15	85	42	58
	214.7			43	11	0	0	2	0	44	53	16	19	12	15	85	29	71
J3	4061.9	Longmaxi (S_1l)	Black shale	43	7	0		0	0	50	43	26	21	10	10	90	42	58
	4064.9			38	7	0	2	0	0	53	37	27	23	13	10	90	39	61
	4068.4			42	7	0	1	0	0	50	41	28	18	13	10	90	43	57
	4071.2			39	7	0	3	0	0	51	42	23	23	12	15	85	50	50
	4075.2			49	6	0	3	0	0	42	45	15	27	13	10	90	26	74
	4079.8			50	8	9	6	0	0	27	42	29	17	12	10	90	43	57
	4083.0			37	13	0	4	0	0	46	39	13	28	20	10	90	38	62
	4086.3			62	5	0	3	0	5	25	58	15	18	9	10	90	23	77
	4089.9			48	6	12	2	0	14	18	55	16	23	6	15	85	42	58
	4092.0			72	2	3	2	0	3	18	56	18	19	7	10	90	44	56
	4095.1			45	5	0	5	0	1	44	48	23	19	10	10	90	27	73

Note: Q–quartz, Pl–plagioclase, Ca–calcite, Py–pyrite, Si–siderite, A–ankerite, Cl–clay, I– illite, C–chlorite, S–smectite.

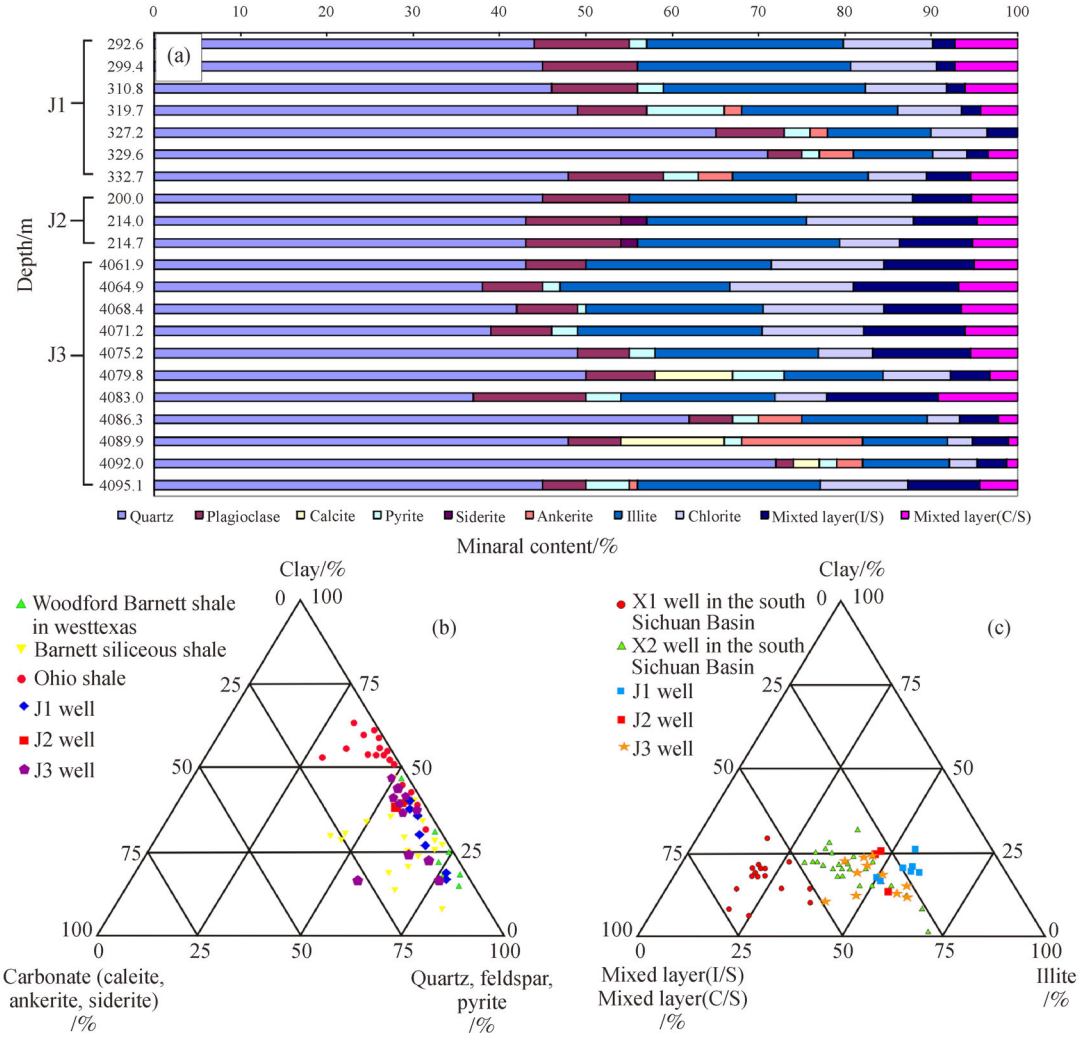

Fig. 3 Bar chart and triangular diagram of mineral components: (a) mineral composition bar chart of shale in J1, J2, and J3; (b) mineral composition triangular chart of marine shale in J1, J2, and J3 and other wells abroad; (c) clay mineral composition triangular chart of marine shale in J1, J2 and J3 as well as wells from the Dianqianbei area.

muddy, siliceous, silty, and calcareous shales. Grapholites can be found in all of the shale lithofacies, so a grapholite shale is not included in this paper. Graptolite fossils are abundant, and they vary in shapes, textures, and lengths. These fossils are distributed in the bedding plane of the shale (Fig. 4(a)), with gradually decreasing content from the bottom up.

Muddy shale mainly developed in the lower part of the Longmaxi Formation. This shale was deposited in an abyssal sea with an enclosed environment, and it often has horizontal bedding. The mud content exceeds 90%, with minor amounts of arenite and pyrite (Figs. 4(b) and 4(c)). Siliceous shale mainly developed in the Wufeng Formation and at the bottom of Longmaxi Formation. This shale is mainly deposited in the deep shelf environment, and the SiO_2 content of siliceous shale ranges from 50% to 72% (Fig. 4(d)). Fossils, such as radiolaria and sponge spicules, are commonly seen in the microscopic thin sections of siliceous shale (Fig. 4(e)). These fossils provide evidence that the silicon source is related to siliceous organisms. Silty shale mainly developed in the middle and upper part of the Longmaxi Formation, with a grayish black or dark gray coloration and horizontal bedding, forming in the shallow shelf environment. The bright laminas are mainly composed of silt, and the dark laminas are mainly composed of mudstone (Fig. 4(f)). Debris particles account for approximately 15%–40% of the material observed and are mainly quartz floating among clay minerals, of medium roundness, and poorly sorted (Fig. 4(g)). Carbonaceous shale is black and gray, (Fig. 4(h)), mainly developed in the lower part of the Longmaxi Formation and was deposited in a hemi-pelagic environment. Carbonaceous shale is mainly composed of clay minerals, quartz, mica, and feldspar containing pyrite and calcite. Quartz grains float among clay minerals and are sub-angular to sub-rounded and poorly sorted (Fig. 4(i)).

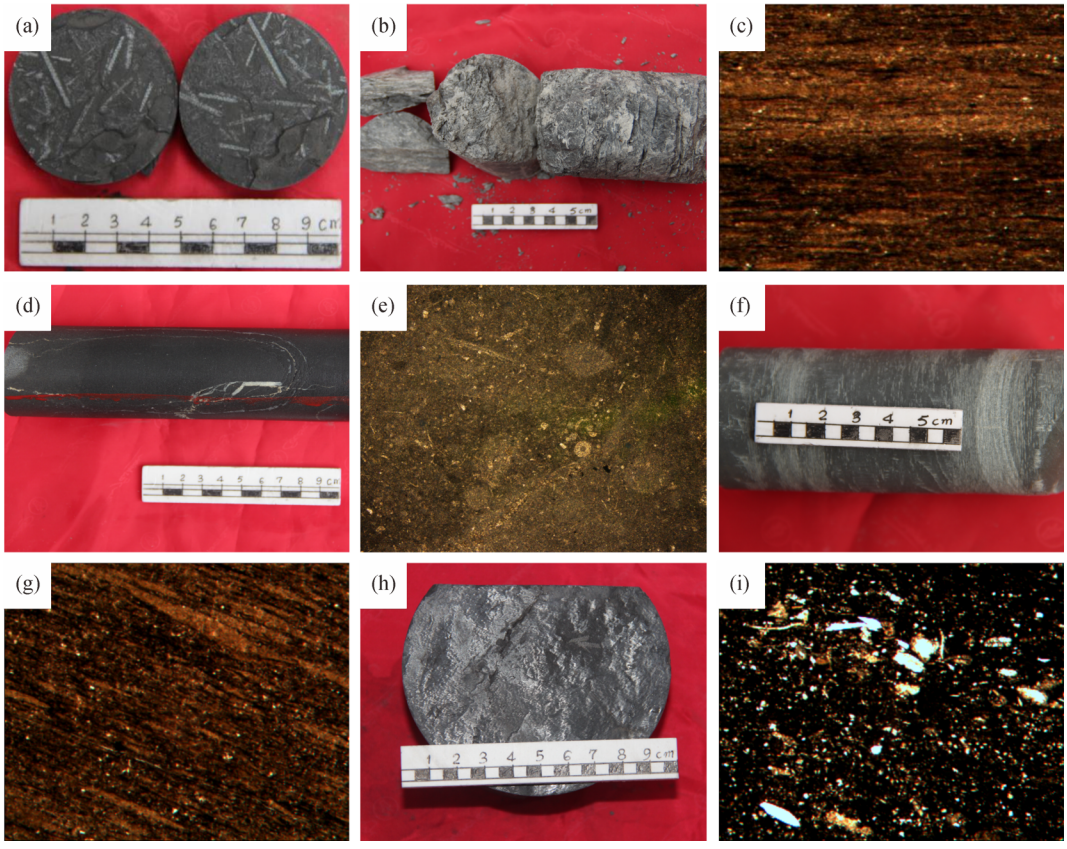

Fig. 4 Photomacrographs and photomicrographs of core lithologic characteristics: (a) Graptolite fossils are well-developed in black shale, Wufeng Formation, 329.0 m; core photo, J1; (b) Muddy shale, 285.3 m, J1; (c) Microscopic photo of muddy shale, mud > 90%, arenite (5%–8%), pyrite > 1%, Longmaxi Formation, 285.3 m, (-) 50×, J1; (d) Siliceous shale, high-angle fractures filled by calcite, 263.2 m, J2; (e) Microscopic photo of siliceous shale, containing numerous radiolaria and sponge spicule fossils, (-) 50×, 263.2 m, J2; (f) Silty shale, 135.4 m, J2; (g) Microscopic photo of silty shale and quartz grains floating among clay minerals, (-) 50×, 135.4 m, J2; (h) Carbonaceous shale, 4064.5 m, J3; (i) Microscopic photo of carbonaceous shale, rich in organic matters, 4064.5 m, J3.

4.3 Organic geochemistry

4.3.1 Kerogen type

Characteristics of kerogen macerals of the six shale samples in J3 well reflect that the kerogen type of shale in the lower part of the Longmaxi Formation is type II_1 (Table 2). Amorphous sapropelinite is the most abundant maceral group, followed by inertinite. Exinite and vitrinite are unnoticeable. The amorphous sapropelinite and inertinite contents are 56.0%–71.0% (average, 64.0%) and 29.0%–54.0% (average, 36.0%), respectively (Table 2). Transmitted light microscopy shows amorphous sapropelinite as yellow or brown with cotton wool or granular structure. Fluorescence microscopy shows amorphous sapropelinite as black or blackish-brown particles. Transmitted light and fluorescence microscopy display inertinite as black and opaque particles (Fig. 5). Amorphous sapropelinite is mainly formed from degradation of algae and other lower aquatic organisms (Tu et al., 1998).

4.3.2 Organic matter maturity and content

Organic matter maturity and organic material content can be used to predict the potential of a source rock. Thus, these factors can be used to indicate organic origin gas in a shale reservoir system (Jarvie et al., 2003; Pu, 2008). VRr ranges from 1.0% to 4.0% of gas shale in the USA. Hence, shale is considered to be in the mature, high-mature, and post-mature phases (Zou et al., 2014). The TOC mass fraction in gas shales usually exceeds 2.0% of the leading shale gas in North America (Curtis, 2002; Burnaman et al., 2009).

The equivalent VRr in the Wufeng Formation as well as the lower part of the Longmaxi Formation ranges from 1.94% to 3.51% (average, 2.66%) (Table 2). This result indicates the maturity level of the dry gas phase. TOC contents of the 48 core samples in the Wufeng Formation and the lower part of the Longmaxi Formation range from 0.22% to 6.15% (average, 3.39%). TOC contents of 39/48 samples (81.25%) exceed 2% (Table 2). The eight other shale samples from J1 have relatively low TOC contents

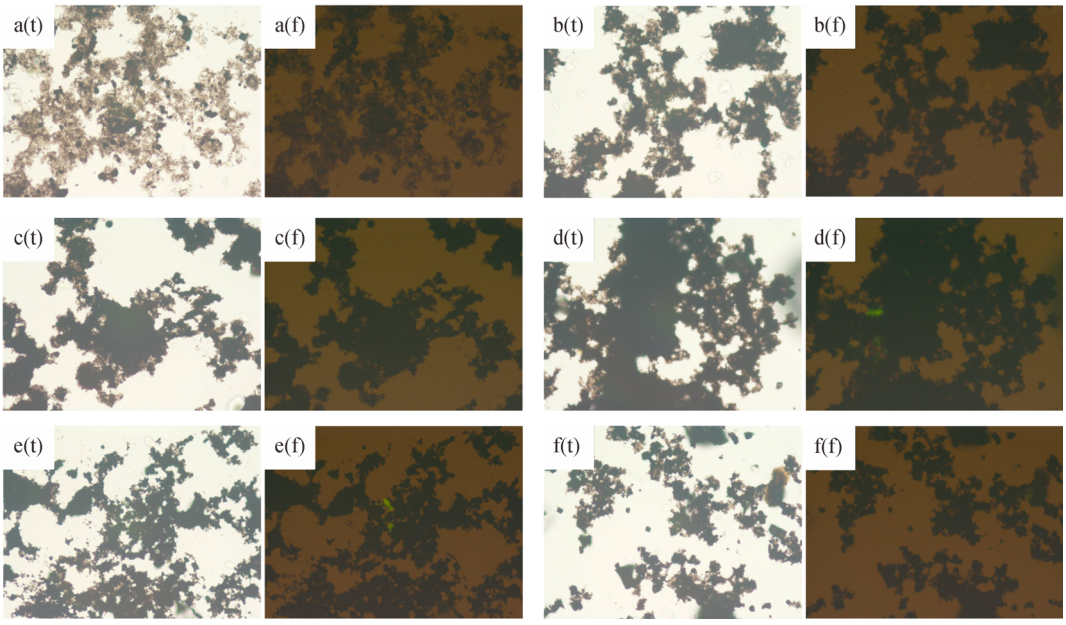

Fig. 5 Kerogen macerals of 6 shale samples in the Longmaxi Formation in the J3 well: [a(t)] Photo by transmitted light microscopy, 4061.91 m; [a(f)] Photo by fluorescence microscopy, 4061.91 m; [b(t)] Photo by transmitted light microscopy, 4071.17 m; [b(f)] Photo by fluorescence microscopy, 4071.17 m; [c(t)] Photo by transmitted light microscopy, 4077.30 m; [c(f)] Photo by fluorescence microscopy, 4077.30 m; [d(t)] Photo by transmitted light microscopy, 4083.04 m; [d(f)] Photo by fluorescence microscopy, 4083.04 m; [e(t)] Photo by transmitted light microscopy, 4088.60 m; [e(f)] Photo by fluorescence microscopy, 4088.60 m; [f(t)] Photo by transmitted light microscopy, 4096.00 m; [f(f)] Photo by fluorescence microscopy, 4096.00 m.

Table 2 Organic geochemistry characteristics of the Wufeng–Longmaxi Formations in the J1 and J3 wells

Well name	Depth/m	Formation	Lithology	TOC/%	VRr/%	Kerogen macerals content/%		Kerogen type
						Sapropelic amorphogen	Inertinite	
J1	292.6	S_1l	Black Shale	0.8	1.95	/	/	/
	300.8	S_1l		0.76	/	/	/	/
	303.5	S_1l		0.83	/	/	/	/
	308.9	S_1l		0.22	/	/	/	/
	310.8	S_1l		0.99	/	/	/	/
	317.4	S_1l		1.59	1.94	/	/	/
	319.7	S_1l		1.28	/	/	/	/
	324.2	S_1l		1.57	/	/	/	/
	327.2	S_1l		3.78	1.96	/	/	/
	329.6	O_3w		2.53	1.99	/	/	/
	332.7	O_3w		4.78		/	/	/
	336.9	O_3w		4.31	2.01	/	/	/
J3	4061.6	S_1l	Black Shale	2.25	/	/	/	/
	4061.9	S_1l		2.99	/	67	33	II_1
	4063.3	S_1l		2.71	/	/	/	/
	4064.9	S_1l		2.98	/	/	/	/
	4065.8	S_1l		2.57	/	/	/	/
	4066.7	S_1l		2.9	/	/	/	/
	4068.4	S_1l		2.03	/	/	/	/

(*Continued*)

Well name	Depth/m	Formation	Lithology	TOC/%	VRr/%	Kerogen macerals content/%		Kerogen type
						Sapropelic amorphogen	Inertinite	
	4069.5	S_1l		1.8	/	/	/	/
	4070.1	S_1l		2.84	2.96	/	/	/
	4071.2	S_1l		3.02	2.68	70	30	II_1
	4071.8	S_1l		3.48	/	/	/	/
	4072.9	S_1l		3.94	/	/	/	/
	4073.7	S_1l		4.2	3.28	/	/	/
	4075.2	S_1l		3.65	3.51	/	/	/
	4076.1	S_1l		3.78	2.82	/	/	/
	4077.3	S_1l		2.87	3.01	63	37	II_1
	4077.8	S_1l		3.58	/	/	/	/
	4079.8	S_1l		3.39	/	/	/	/
	4080.8	S_1l		4.79	2.96	/	/	/
	4081.5	S_1l		4.1	/	/	/	/
	4082.6	S_1l		4.64	/	/	/	/
	4083	S_1l		4.83	/	71	29	II_1
	4084.1	S_1l		5.54	/	/	/	/
	4086.3	S_1l		4.8	2.87	/	/	/
	4087.2	S_1l		4.65	/	/	/	/
	4087.8	S_1l		4.13	2.73	/	/	/
	4088.6	S_1l		3.98	/	57	43	II_1
	4089.9	S_1l		4.78	2.98	/	/	/
	4090.1	S_1l		4.52	/	/	/	/
	4091	S_1l		6.15	/	/	/	/
	4092	S_1l		5.12	2.64	/	/	/
	4093	S_1l		5.98	2.75	/	/	/
	4095.1	S_1l		5.15	2.82	/	/	/
	4096	S_1l		4.56	/	56	44	II_1
	4096.3	S_1l		3.21	/	/	/	/
	4097.2	S_1l		3.15	/	/	/	/

(0.22%–1.59%; average, 1.00%) (Table 2) because this well is close to the Yichang Uplift. The Yichang Uplift commenced at a time roughly corresponding to the upper Wufeng Formation (~446 Ma) and lasted about 4–7 Ma (Wang et al., 2013). In this period, the area of J1 was an "under water uplift" within a shallow water body (Chen et al., 2001).

4.4 Reservoir space characteristics

4.4.1 Micropore types

Shale contains many microscopic pores that serve as gas reservoirs (Loucks and Ruppel, 2007; Loucks et al., 2009). Microscopic pores in shale have different shapes, sizes, and distributions. The micro/nanometer pore system influences gas accumulation (Chalmers et al., 2012). Pores in shale have been classified as organic or inorganic (Jarvie et al., 2007; Reed and Loucks, 2007; Slatt and O'Brien, 2011). Organic pores are generated during maturation and hydrocarbon expulsion (mass deficit). Pores can be classified as clay mineral (Figs. 6(a)–6(d)), intercrystalline (Fig. 6(e)), mineral moldic (Fig. 6(f)), dissolution (Fig. 6(g)), and organic matter (Fig. 6(h)) pores on the basis of their genetic types and sizes. Microfractures are also sufficiently developed as shown in the SEM image (Fig. 6(i)).

4.4.2 Petrophysical properties from NMR analyses

The T_2 relaxation time spectra of six core samples before and after centrifugation are shown in Fig. 7, from which T_2

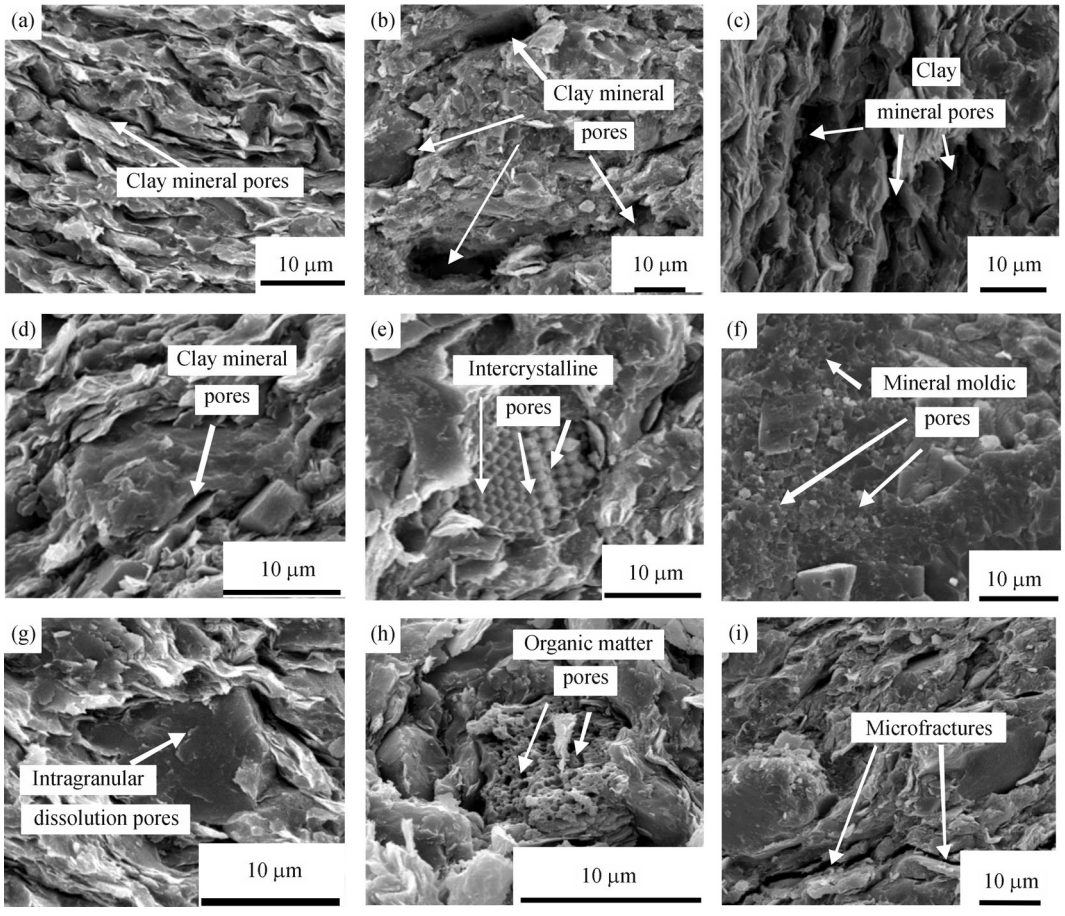

Fig. 6 Types of microscopic pores of rocks in the Wufeng and Longmaxi formations in J1: (a) clay mineral pores, Longmaxi Formation, 297.4 m; (b) clay mineral pores, Wufeng Formation, 329.4 m; (c) clay mineral pores, Longmaxi Formation, 283.2 m; (d) clay mineral pores, Longmaxi Formation, 311.2 m; (e) pyrite intercrystalline pores, Longmaxi Formation, 127.7 m; (f) mineral moldic pores, Longmaxi Formation, 325.1 m; (g) dissolution pores, Longmaxi Formation, 301.3 m; (h) organic matter pores, Wufeng Formation, 330.2 m; (i) microfractures, Wufeng Formation, 331.8 m.

Table 3 NMR results of the six core samples from the J1, J2, and J3 wells

Well name	Depth/m	Formation	NMR porosity/%	NMR permeability/md	Bound water saturation/%	Free gas saturation/%	T_2/ms
J1	299.4	S_1l	1.28	0.000033	74.52	25.48	2.23
	333.9	O_3w	1.11	0.00005	64.29	35.71	1.55
J2	200.0	S_1l	2.31	0.000225	78.45	21.55	2.23
	214.7	S_1l	1.97	0.00033	68.7	31.3	1.55
J3	4068.4	S_1l	2.99	0.0022	65.93	34.07	2.23
	4092.2	S_1l	4.41	0.00085	87.22	12.78	4.64

cutoff values are obtained. These values show that the porosity obtained from the NMR tests ranges from 1.11% to 4.41%, (average, 2.35%). The measured permeability ranges from 0.00003 md to 0.0022 md (average, 0.000615 md). Bound water saturation ranges from 64.29% to 87.22% (average, 73.19%). Free gas saturation ranges from 12.78% to 35.71% (average 26.82%) (Table 3). These results show that the gas shale reservoirs in the Wufeng and Longmaxi formations are characterized by low porosity and extremely low permeability. Permeability is positively correlated with porosity (Fig. 8).

4.5 Gas contents and components

All possible gas storage forms may exist in shale, and these forms are generally classified into free, adsorbed, and dissolved gases (Jarvie et al., 2003; Martini et al., 2003; Montgomery et al., 2005). Water immersion experiments

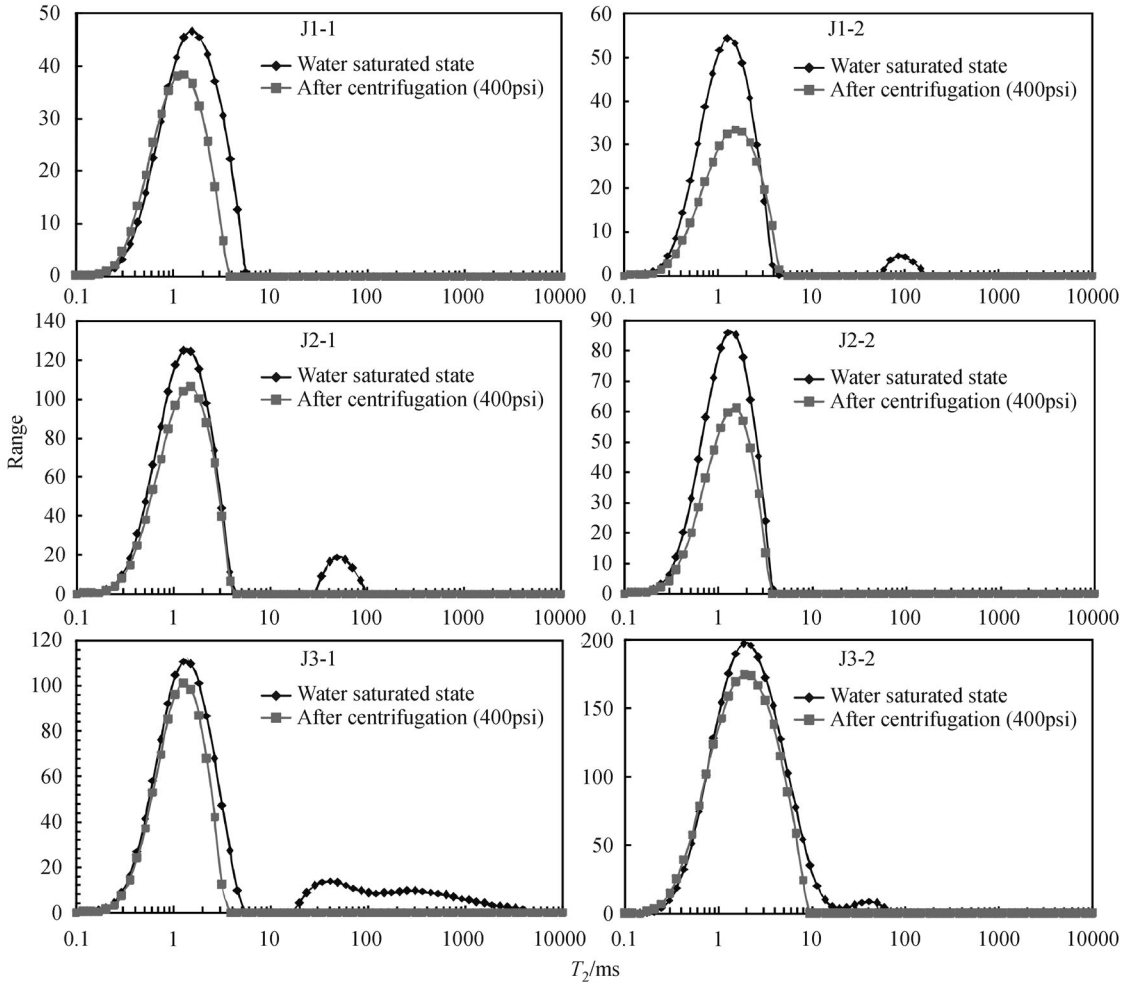

Fig. 7 NMR T_2 relaxation time spectrum before and after centrifugation of core samples.

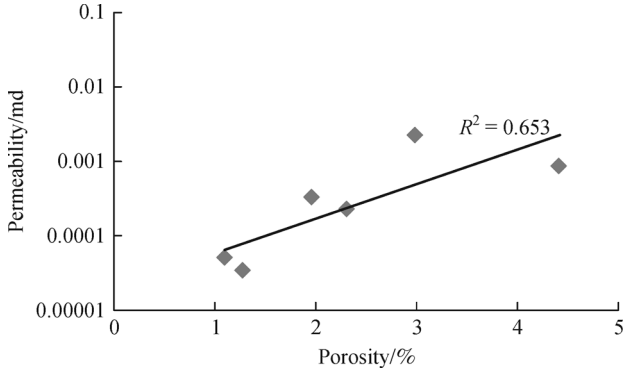

Fig. 8 Relationship of NMR permeability and NMR porosity of core samples.

on the fresh cores show the existence of shale gas. The 12 black shale samples from the lower part of the Longmaxi Formation in J3 generally have high gas content, i.e., 1.12–3.16 m^3/t (average 2.15 m^3/t; Table 4). However, four shale samples from the J1 well show low gas contents, i.e. 0.12–0.5 m^3/t (average 0.23 m^3/t) because the shallow depth of this well allows gas to escape to the atmosphere (Table 4).

Component analysis of the 16 canisters of the separated gas indicates that gas from J1 in the Longmaxi Formation is mainly composed of nitrogen with low methane content. Meanwhile, gases from J1 in the Wufeng Formation and J3 in the Longmaxi Formation are mainly composed of methane (Table 5). Three gas samples from J1 contain 92.38%–97.33% nitrogen (average 95.38%). The methane content of these samples only ranges from 0.73% to 3.04% (average 2.73%). Only one gas sample from J1 in the Wufeng Formation has a high methane content of 85.31% and nitrogen content of 13.89%. Twelve gas samples from J3 contain 90.64%–96.54% methane (average 93.48%).

The high nitrogen content from J1 in the Longmaxi Formation can be attributed to exhumation. Shallow rock formations are generally located in a gas–water exchange

Table 4 Separation result of the shale gas content in the J1 and J3 wells

Well name	Depth/m	Formation	TOC/%	Lost gas /($m^3 \cdot t^{-1}$)	Separated gas /($m^3 \cdot t^{-1}$)	Residual gas /($m^3 \cdot t^{-1}$)	Total gas /($m^3 \cdot t^{-1}$)
J1	292.6	S_1l	0.8	0	0	0.12	0.12
	310.8		0.99	0	0.01	0.08	0.09
	319.7		1.28	0	0.02	0.2	0.22
	332.7	O_3w	2.53	0.03	0.18	0.29	0.5
J3	4061.9	S_1l	2.99	0.67	0.43	0.05	1.14
	4064.9		2.98	0.97	0.66	0.04	1.68
	4068.4		2.03	0.66	0.4	0.06	1.12
	4071.2		3.02	0.65	0.58	0.07	1.3
	4073.7		4.2	0.97	0.94	0.02	1.93
	4075.2		3.65	0.91	0.41	0.11	1.43
	4079.8		3.39	2.08	1.03	0.06	3.16
	4083.0		4.83	1.73	1.06	0.09	2.88
	4086.3		4.8	2.49	1.37	0.06	3.93
	4089.9		4.78	0.86	0.49	0.07	1.43
	4091.0		6.15	1.8	1.01	0.05	2.87
	4095.1		5.15	1.64	1.17	0.17	2.98

Table 5 Component analysis of shale gas in the J1 and J3 wells

Well name	Depth /m	He /%	H_2 /%	O_2 /%	N_2 /%	Co_2 /%	H_2s /%	C_1 /%	C_2 /%	C_3 /%	Ic_4 /%	Nc_4 /%	Ic_5 /%	Nc_5 /%	C_6+ /%
J1	292.6	0	0	0	97.33	1.56	0	0.94	0.02	0.03	0.02	0.04	0.02	0.03	0.01
	310.8	0	0	0	96.43	2.77	0	0.73	0.01	0.01	0.01	0.02	0.01	0.01	0
	319.7	0	0	0	92.38	0	0	7.46	0.07	0.02	0.01	0.03	0.01	0.02	0
	332.7	0.03	0.01	0	13.89	0.71	0	85.31	0.05	0	0	0	0	0	0
J3	4061.9	0.05	0.31	0	0	3.4	0	96.16	0.08	0	0	0	0	0	0
	4064.9	0.05	0.02	0	0	5.53	0	94.37	0.03	0	0	0	0	0	0
	4068.4	0.04	0.12	0	0	3.22	0	96.54	0.08	0	0	0	0	0	0
	4071.2	0.03	0.89	0	0.06	3.52	0	95.39	0.11	0	0	0	0	0	0
	4073.7	0.04	0.96	0	4.5	3.3	0	91.07	0.13	0	0	0	0	0	0
	4075.2	0.07	0	0	1.86	7.37	0	90.64	0.06	0	0	0	0	0	0
	4079.8	0.01	0	0	6.56	2.08	0	91.2	0.15	0	0	0	0	0	0
	4083.0	0.05	0	0	6.25	1.01	0	92.64	0.05	0	0	0	0	0	0
	4086.3	0.03	0	0	4.6	0.88	0	94.4	0.09	0	0	0	0	0	0
	4089.9	0.02	0	0	4.71	3.27	0	91.94	0.06	0	0	0	0	0	0
	4091.0	0.02	0.02	0	4.72	3.21	0	91.97	0.06	0	0	0	0	0	0
	4095.1	0.03	0	0	1.87	2.6	0	95.38	0.12	0	0	0	0	0	0

zone in which nitrogen and oxygen in the air come from the formation water. Oxygen is easier to consume during oxidation compared with other substances. Thus, nitrogen accumulates and is preserved over time, leading to high nitrogen contents in rock formations close to the surface.

5 Discussion

5.1 Relationship between TOC and minerals

We found a weakly positive correlation between TOC content and quartz and a weakly negative correlation

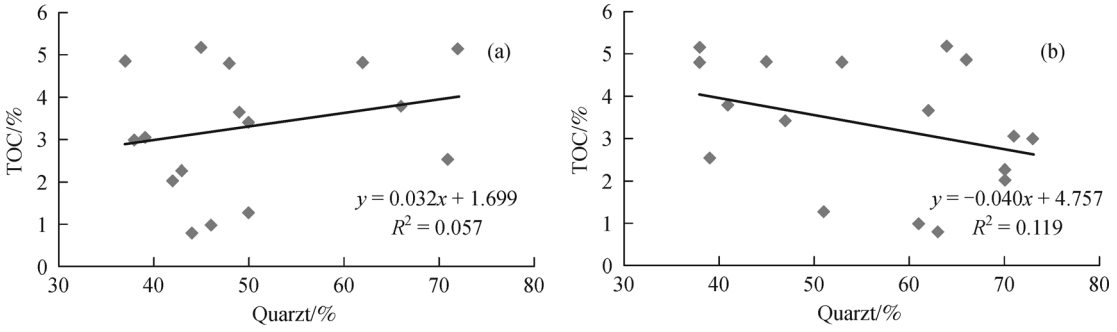

Fig. 9 Relationships among clay minerals, quartz, and TOC of black shale in J1 and J3. Relationship between (a) clay mineral content and TOC and (b) quartz content and TOC.

between TOC and clay minerals (Fig. 9). Authigenic quartz is the main silicon mineral in marine shale (Fu et al., 2011). Thus, the higher the quartz content, the higher the silicon content. Silicon provides evidence of a hydrothermal sedimentary environment in situ. This environment provides the formation conditions and storage space for organic matter such as radiolarian, sponge (Fig. 4 (e)), and fung us algae fossils (Xie et al., 2013), which can increase the TOC content of shale

5.2 Relationship between TOC and total gas content

Strapoc et al. (2010) reported a strong positive correlation between TOC and total gas content in Owen and Pike Counties, Indiana (Devonian–Mississippian New Albany Shale, eastern Illinois Basin). In the current study, we examined the correlation between total gas content from the canister desorption of fresh cores and TOC content (Fig. 10). Results showed that TOC content of gas shale reservoirs is positively correlated with the total gas content. Hence, gas content increases with increasing TOC content, which indicates that organic matter content is primarily responsible for total gas content in the study shale.

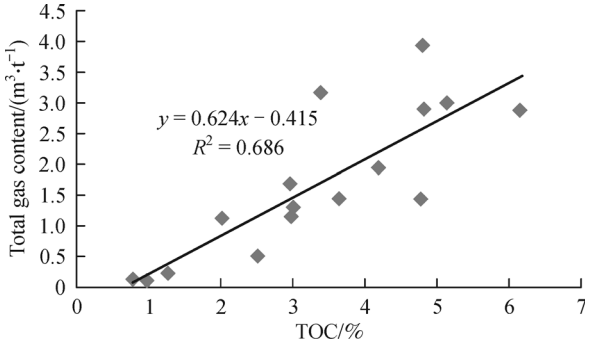

Fig. 10 Correlation of total gas content and TOC in the J1 and J3 wells.

5.3 Factors controlling methane adsorption capacity of shale

Free gas is mainly stored in the large pores or fractures of shale, facilitating exploitation of this gas. However, shale gas primarily exists in an adsorbed state on the surface of clay minerals and organic matter nanopores (Curtis, 2002). Adsorbed gas content of organic-rich shale in North America ranges from approximately 20% to 85% (Curtis, 2002). Mavor (2003) reported that the adsorbed gas content of Barnett shale is about 60% of the original shale gas geological reserves. The adsorbed gas content of shale was inferred to exceed 40% (Lu et al., 1995; Montgomery et al., 2005; Li et al., 2007; Wu et al., 2012). Therefore, investigating the factors that control methane adsorption capacity of shale should be investigated.

Ten core shale samples from the Wufeng Formation and lower part of Longmaxi Formation were investigated by analyzing the methane adsorption isotherms. Langmuir volume (V_L) of all samples ranges from 1.71 m^3/t to 4.33 m^3/t (Table 6; average 3.01 m^3/t). This result indicates the high adsorption capacity of shale. Langmuir pressure (P_L) of the ten samples ranges from 1.49 MPa to 3.44 MPa (Table 6; average 2.12 MPa). This result reveals that the adsorption isotherms take the shape of relatively flat curves (Fig. 11).

Organic matter thermal maturation and mineral component can significantly affect gas adsorption in shales (Li et al., 2007; Ross and Bustin, 2009; Wu et al., 2012; Zhang et al., 2012; Gao et al., 2013). A general positive correlation of CH_4 sorption capacity with TOC in shale has been observed in previous studies (Lu et al., 1995; Ross and Bustin, 2007; Cui et al., 2009). We investigated the effects of TOC, organic maturity, and mineral components on methane adsorption capacity of the gas shales to study these controlling factors on adsorption capacity of methane from the Wufeng and Longmaxi formations. Methane adsorption capability is positively correlated with TOC content and organic maturity

Table 6 Sample data from the isothermal adsorption test of shale methane (30°C)

Well name	Sample name	Depth /m	Fitting coefficient	V_l /($m^3 \cdot t^{-1}$)	P_l /MPa	TOC /%	VRr /%	Clay /%	Quartz /%
J1	J1-1	292.6	0.9968	1.71	1.49	0.8	1.95	43	44
	J1-2	310.8	0.9982	2.26	1.53	0.99	/	41	46
	J1-3	327.2	0.9954	3.02	3.08	3.78	1.96	21	66
	J1-4	329.6	0.9991	2.35	2.36	2.53	1.99	19	71
J3	J3-1	4064.9	0.9993	2.88	3.44	2.98	/	38	53
	J3-2	4071.2	0.9991	3.34	1.74	3.02	2.68	39	51
	J3-3	4079.8	0.9992	3.34	2.02	3.39	/	27	50
	J3-4	4086.3	0.9996	4.33	2.1	4.8	2.87	25	62
	J3-5	4092	0.9998	4.00	1.91	5.12	2.64	18	72
	J3-6	4095.1	0.9996	2.82	1.49	5.15	2.82	44	45

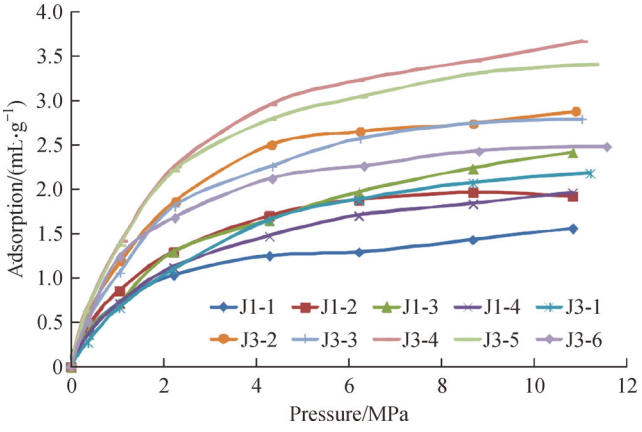

Fig. 11 Isothermal curves for 10 black shale samples from the J1 and J3 wells.

(Fig. 12). The reasons for these phenomena have been extensively explained in other studies (Lu et al., 1995; Li et al., 2007; Ross and Bustin, 2007,2009 ; Cui et al., 2009; Wu et al., 2012; Zhang et al., 2012; Gao et al., 2013).

We investigated the relationships between adsorption capability and the clay and quartz contents of shale, given that the total clay and quartz contents account for > 75% of the whole shale minerals (Table 1). We found a weakly positive correlation between adsorption capability of shale and quartz content (Fig. 13(a)), contrary to the weakly negative correlation between adsorption capability and clay content (Fig. 13(b)). This result is consistent with that reported by Gao et al. (2013). Thus, from the results in Section 5.1, a weakly positive correlation exists between TOC content and quartz content, and a weakly negative correlation exists between TOC and clay mineral content.

5.4 Comparison with commercial shale gas

The petrology, mineralogy, thickness, organic geochemistry, and physical properties of black shale from the Upper Ordovician Wufeng Formation and the Lower Silurian Longmaxi Formation located north of the mid-Yangtze area were examined through the techniques mentioned in Section 1. Moreover, we compared the characteristics of a gas shale reservoir with gas shale basins in these areas to commercial shale gas-producing areas in the upper Yangtze area (Table 7) (Guo, 2014; Guo and Zhang, 2014; Zou et al., 2014).

The lithology of the high-quality part of the Upper

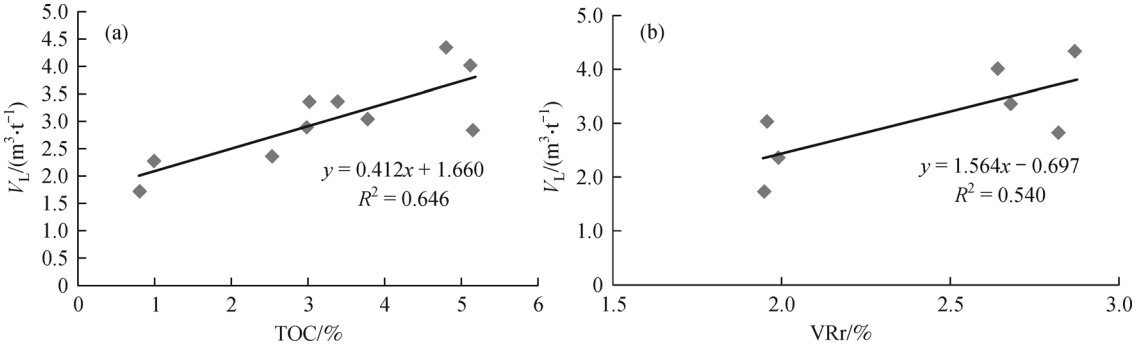

Fig. 12 Relationships among TOC, VRr, and methane adsorption capability of black shale in J1 and J3: (a) TOC and V_L and (b) VRr and V_L.

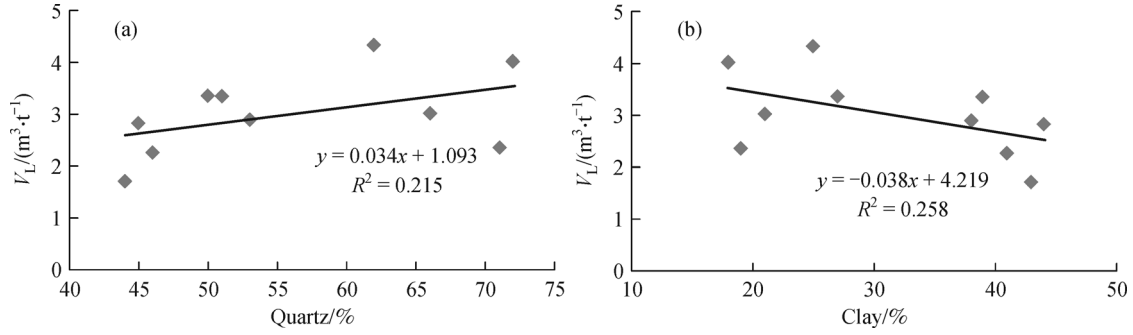

Fig. 13 Relationships among quartz, clay, and methane adsorption capability of black shale in J1 and J3: (a) Quartz content and adsorption capability and (b) clay content and adsorption capability.

Table 7 The comparison of gas shale reservoir characteristics among the study area, gas shale basins in America, and domestic commercial shale gas producing areas

Area	Formation	Lithology	Brittle mineral/%	Clay mineral/%	Porosity /%	Permeability /($\times 10^{-3}$μm^2)	Shale thickness/m	TOC /%	Kerogen type	VRr /%	Reservoir Space
Jiaoshiba	Wufeng-Longmaxi	Carbonaceous shale Siliceous shale	33.9–80.3 (56.5)	16.6–62.8 (40.9)	1.17–8.61 (4.87)	0.0001–335.21	39.5–89	0.46–7.13 (2.66)	I, II_1	2.42–2.8 (2.59)	Matrix Pores + Facture
Chang-ning	Wufeng-Longmaxi	Siliceous shale Calcareous shale	Quartz17–58(33) Feldspar3–18(7) Calcite + dolomite 4–65(22)	10–53 (31)	3.4–8.2 (5.4)	0.000 22–0.0019 (0.00029)	40–60	1.9–7.3 (4)	I, II_1	2.3–2.8 (2.5)	Matrix Pores + Facture
Weiyuan	Wufeng-Longmaxi	Siliceous shale Calcareous shale argillaceous shale	Quartz17–58(33) Feldspar3–18(7) calcite + dolomite 4–65(22)	15–49 (34)	3.9–6.7 (5.3)	0.000015–0.000090 (0.000 042)	26–50	1.9–6.4 (2.7)	I, II_1	2.7	Matrix Pores + Facture
Fushun–Yong-chuan	Wufeng-Longmaxi	Siliceous shale Calcareous shale	Quartz45–48(47) Feldspar3–9(7) Calcite + dolomite 4–6(5)	37–40 (39)	3.0–7.0 (4.2)	0.000187–0.000 273 (0.000 233)	60–120	1.6–6.8 (3.8)	I, II_1	2.5–3.0	Matrix Pores + Facture
Zhaotong	Wufeng-Longmaxi	Siliceous shale calcareous shale	Quartz24–54(40) feldspar4–5(4.5) calcite + Dolomite 0–44(22)	23–42 (32)	2.6–7.0 (5.9)	0.0043–0.042 (0.019)	30–40	1.6–4.9 (3.2)	I, II_1	2.1–3.0	Matrix Pores + Facture
The study area	Longmaxi	Carbonaceous shale siliceous shale	Quartz37–72(48) feldspar2–13(8.2) calcite + Dolomite 0–26(3.5)	18–53 (37.41)	1.11–4.41 (2.35)	0.00003–0.0022 (0.000615)	48–55	0.22–6.15 (3.39)	II_1	1.94–3.51 (2.66)	Matrix Pores + Facture

Data source: Guo, 2014; Guo and Zhang, 2014; Zou et al., 2014.

Ordovician–Lower Silurian region (Wufeng and Longmaxi formations) is mainly carbonaceous and siliceous shale, similar to the Jiaoshiba area. Calcareous shale in the study area is rarer than that in other commercial shale gas-producing areas, that is, the sedimentary environment in the study area is more closed than in other areas. The thickness of the high-quality shale is relatively large. Specifically, high-quality shale is thicker in the study area than those in the Changning, Weiyuan, and Zhaotong areas, but similar to or slightly thinner than that in the Jiaoshiba and Fushun areas. The total average content of quartz, feldspar, and pyrite is 63.0% (48.0% quartz). In addition, the brittle mineral content is relatively high, which is similar to that in other areas. Shale in the study area is type II_1 kerogen, compared with types I and II_1 in all other areas. VRr ranges from 1.94% to 3.51%, similar to other areas. TOC content is 0.22%–6.15%, (average 3.39%), which is relatively high compared with all of the shale gas-producing areas surveyed. The shale reservoir space includes mainly matrix pores and fractures. The reservoir exhibits low porosity and extremely low permeability, similar to that in the upper Yangtze area. However,

its porosity is only slightly less than those of other areas. Furthermore, its permeability is superior to those of Weiyuan, Fushun-yongchuan, and Changing areas. These results indicate that the northern region of the middle Yangtze area may be a good shale gas resource.

6 Conclusions

1) High-quality black shale was developed in the Wufeng Formation and lower part of the Longmaxi Formation during the late Katian to the early Rhuddanian. Black shale layers in the J1, J2, and J3 wells in the Wufeng Formation and the lower part of the Longmaxi Formation are 54.88 m, 48.49 m, and 52.00 m thick, respectively. The rock mainly comprises carbonaceous and siliceous shales intercalated with silty shale. The thickness of the black shale and lithology are similar to those of gas shale basins in other commercial shale gas-producing areas. The average clay and brittle mineral contents in black shale are 37.5% and 62.5% (48.9% quartz), respectively. Brittle mineral content is relatively high.

2) Shale in the Wufeng Formation and in lower part of the Longmaxi Formation has type II_1 kerogen. VRr is 1.94%–3.51% (average 2.66%). This result indicates a mature level of dry gas phase. TOC content of the Wufeng and Longmaxi formations ranges from 0.22% to 6.15% (average 3.39%). This result shows high level among all shale gas-producing areas.

3) Microscopic pores can be classified into clay mineral, intercrystalline, mineral moldic, dissolution, and organic matter pores on the basis of the genetic types and sizes of the pores. Microfractures are sufficiently developed. Shale reservoir of the Wufeng and Longmaxi formations is characterized by low porosity (1.11%–4.41%; average 2.35%) and extremely low permeability (0.00003–0.0022 md; average 0.000615 md). However, its porosity is only slightly lower than those of other areas. Moreover, its permeability is superior to those of Weiyuan, Fushun-yongchuan, and Changing areas in Sichuan Basin.

4) The 12 black shale samples from the lower part of Longmaxi Formation in J3 have generally high gas contents, i.e., 1.12–3.16 m^3/t (average 2.15 m^3/t). The gas is mainly composed of methane. The 12 gas samples contain 90.64%–96.54% methane (average 93.48%).

5) A weakly positive correlation exists between TOC content and quartz, whereas a weakly negative correlation exists between TOC and clay minerals. TOC content of gas shale reservoirs is positively correlated with the total gas content. In addition, TOC, VRr, and mineral presence and content influence the methane adsorption capability of shale. Adsorption capability is positively correlated with TOC content and organic maturity. A weakly positive correlation is found between adsorption capability of shale and quartz content, contrary to the weakly negative correlation of the former and clay content.

Acknowledgements This study was supported by the National Natural Science Foundation of China (Grant No. 41302123), the Doctoral Program of Higher Education (Specialized Research Fund) of China (Grant No. 20125121130001), and the Science Foundation of Education Department of Sichuan Province (Grant No. 13ZB0190).

References

Burnaman M D, Xia W W, Shelton J (2009). Shale gas play screening and evaluation criteria. China Petroleum Exploration, 14(3): 51–64

Chalmers G R, Bustin R M, Power I M (2012). Characterization of gas shale pore systems by porosimetry, pycnometry, surface area, and Field emission scanning electron microscopy / transmission electron Microscopy image analyses: Examples from the Barnett, Woodford, Haynesville, Marcellus, and Doigunits. AAPG Bull, 96(6): 1099–1119

Chen W L, Zhou W, Luo P, Deng H C, Li Q, Shan R, Qi M H (2013). Analysis of the shale gas reservoir in the Lower Silurian Longmaxi Formation, Changxin1 well, Southeast Sichuan Basin, China. Yanshi Xuebao, 29(3): 1073–1086 (in Chinese)

Chen X, Rong J, Li Y, Boucot A J (2004). Facies patterns and geography of the Yangtze region, South China, through the Ordovician and Silurian transition. Palaeogeogr Palaeoclimatol Palaeoecol, 204(3-4): 353–372

Chen X, Rong J Y, Zhou Z Y, Zhang Y D, Zhan R B, Liu J B, Fan J X (2001). Qianzhong Uplift and Yichang Uplift from Ordovician to Silurian in Yangtze area. Chin Sci Bull, 46(12): 1052–1056

Cui X, Bustin A M, Bustin R (2009). Measurements of gas permeability and diffusivity of tight reservoir rocks: different approaches and their applications. Geofluids, 9(3): 208–223

Curtis J B (2002). Fractured shale-gas systems. AAPG Bull, 86(11): 1921–1938

Fu X D, Qin J Z, Teng G E, Wang X F (2011). The Mineral components of the source rocks and their petroleum significance: a case from Paleozoic Marine source rocks in the Middle and Upper Yangtze region. Journal of petroleum Exploration and Development, 38(6): 671−684 (in Chinese)

Fu Y X, Zhang P, Li Z X, Yang Z W, Liu X M, Wang S H (2007). The tectonic characteristics and their significance for hydrocarbon exploration in mid- Yangtze area. Geotectonica Et Metallogenia., 31(3): 308–314 (in Chinese)

Gao H Q, Cao H H, Ding A X, Gong Y, Li C, Ye J G, Yue X J (2013). Isotherm adsorption characteristic of marine and continental shale and its controlling factors. Natural Gas Geoscience, 24(6): 1290–1297 (in Chinese)

Guo T L, Zhang H R (2014). Formation and enrichment mode of Jiaoshiba shale gas field, Sichuan Basin. Petroleum Exploration and Development, 41(1): 31–40 (in Chinese)

Guo X S (2014). The Enrichment Mechanism and Exploration Technology of Shale Gas in Jiaoshiba Area, Fuling.Beijing: Science Publishing House, 1–347 (in Chinese)

Jarvie D M, Hill R J, Pollastro R M, Wavrek D A, Bowker K A, Claxton B L, Tobey M H (2003). Evaluation of unconventional natural gas prospects: The Barnett Shale fractured shale gas model. In: European Association of International on Organic Geochemistry Meeting, Poland, September 8–12, Krakow

Jarvie D M, Hill R J, Ruble T E, Pollastro R M (2007). Unconventional Shale gas systems: the Mississippian Barnett Shale of north Central Texas as one model for thermogenic shale gas assessment. AAPG Bull, 91(4): 475–499

Kang Y Z (2012). Characteristics and exploration prospect of unconventional shale gas reservoirs in China. Natural Gas Industry, 32(4): 1–5 (in Chinese)

Li A G, Wang F Y (2001). Accumulating gas system in Shizhu area of eastern Chongqing. Petroleum exploration and development, 28(6): 20–22 (in Chinese)

Li X J, Hu S Y, Cheng K M (2007). Suggestions from the Development of fractured shale gas in North America. Journal of Petroleum Exploration and Development, 34(4): 392–400 (in Chinese)

Li Y X, Lin J H, Long Y K, Li J H, Zhang L Y (2011). Exploration prospect of gas-bearing marine mudstone-shale in Lower Palaeozoic in the central Yangtze area, China. Geological Bulletin of China, 30 (2/3): 349–356 (in Chinese)

Liu S G, Ma W X, Luba J, Huang W M, Zeng X L, Zhang C J (2011). Characteristics of the shale gas reservoir rocks in the Lower Silurian Longmaxi Formation, East Sichuan Basin, China. Acta Petrologica Sinaca, 27(8): 2239–2252 (in Chinese)

Liu X M, Fu Y X, Guo Z F, Wang Y L, Liang X W (2009). Characteristics of basin evolution and hydrocarbon response in the middle Yangtze region since Nanhua period. Petroleum Geology and Experiment, 31(2): 160–165 (in Chinese)

Long Y K (2011). Lower Palaeozoic shale gas exploration potential in the central Yangtze area, China. Geological Bulletin of China, 30(2/3): 344–348 (in Chinese)

Loucks R G, Reed R M, Ruppel S C, Jarvie D M (2009). Morphology, genesis and distribution of nanometer scale pores in siliceous Mudstones of the Mississippian Barnett shale. J Sediment Res, 79 (12): 848–861

Loucks R G, Ruppel S C (2007). Mississippian Barnett shale: lithofacies and depositional setting of a deep water shale gas Succession in the Fort Worth basin, Texas. AAPG Bull, 91(4): 579–601

Lu X C, Li F C, Watson A T (1995). Adsorption measurements in Devonian shales. Fuel, 74(4): 599–603

Ma L, Chen H J, Gan K W, Xu K D, Xu X S, Wu G Y, Ye Z, Liang X, Wu S H (2004). South China Tectonics and Marine oil and gas Geology(1). Beijing: Geological Publishing House, 259–364 (in Chinese)

Martini A M, Walter L M, Ku C W, Budai J M, McIntosh J C, Schoell M (2003). Microbial production and modification of gases in sedimentary basins: A geochemical case study from a Devonian shale gas play, Michigan basin. AAPG Bull, 87(8): 1355–1375

Mavor M (2003). Barnett Shale gas-in-place volume including adsorbed and free gas volume. AAPG Southwest Section Meeting, Texas, March 1−4. Fort Worth: Texas

Montgomery S L, Jarvie D M, Bowker K A, Pollastro R M (2005). Mississippian Barnett Shale, Fort Worth Basin, North-central Texas: Gas-shale Play with Multitrillion Cubic Foot Potential. AAPG Bull, 89(2): 155–175

Mu C L, Zhou K K, Liang W, Ge X Y (2011). The depositional environments and petroleum exploration of the Early Paleozoic Hydrocarbon source rocks in the middle and upper Yangtze region. Acta Geol Sin, 30(4): 526–532

Papazis P K (2005). Petrographic characterization of the Barnett Shale, Fort Worth Basin, Texas. M.S. Thesis, University of Texasat Austin, Austin, Texas, 142p and appendices

Pu P L (2008). Analysis of the reservoir forming conditions of shale gas potential in Sichuan basin. Master Degree Thesis. China University of Petroleum, Beijing, 5–6 (in Chinese)

Qin J Z, Fu X D, Shen B J, Liu W X, Teng G E, Zhang Q Z, Jiang Q G (2010). Characteristics of ultramicroscopic organic lithology of excellent marine shale in the Upper product sequence, Sichuan Basin. Petroleum Geology & Experiment, 32(2): 164–170 (in Chinese)

Qiu X S, Yang B, Hu M Y (2013). The Characteristics of shale reservoirs and gas content of Wufeng- Longmaxi Formation in the middle Yangtze region. Journal of Natural Gas Team, 24(6): 1274–1283 (in Chinese)

Reed R M, Loucks R G (2007). Imaging nanoscale pores in the Mississippian Barnett Shale of the northern Fort Worth Basin. AAPG Annual Convention Abstracts 6, 115

Slatt R M, O'Brien N R (2011). Pore types in the Barnett and Woodford Gas shales: Contribution to understanding gas storage and migration Pathways in fine-grained rocks. AAPG Bull, 95(12): 2017–2030

Ross D J K, Bustin R M (2007). Shale gas potential of the Lower Jurassic Gordondale Member, northeastern British Columbia, Canada. Bull Can Pet Geol, 55(1): 51–75

Ross D J K, Bustin R M (2009). The importance of shale composition and pore structure upon gas storage potential of shale gas reservoirs. Mar Pet Geol, 26(6): 916–927

Schoenherr J, Littke R, Urai J L, Kukla P A, Rawahi Z (2007). Polyphase thermal evolution in the Infra-Cambrian Ara Group (South Oman Salt Basin) as deduced by maturity of solid reservoir bitumen. Org Geochem, 38(8): 1293–1318

Shang Z Y, Ou Y J, Feng Q N (1998). The new logging technology and development of reservoir evaluation of oil and gas.Beijing: Petroleum Industry Press, 276 (in Chinese)

Strapoc D, Mastalerz M, Schimmelmann A, Drobniak A, Hasenmueller N R (2010). Geochemical constraints on the origin and volume of gas in the New Albany Shale (Devonian–Mississippian), eastern Illinois Basin. AAPG Bull, 94(11): 1713–1740

Teng J W, Liu Y S (2013). Analysis of distribution, storage potential and prospect for shale oil and gas in China. Progress in Geophysics, 28 (3): 1083–1108 (in Chinese)

Tu J Q, Wang S Z, Fei X D (1998). Discussion on certain problems to the division of organic matter types in kerogen. Experimental petroleum geology, 20(2): 187–191

Wang Y, Rong J Y, Zhan R B, Huang B, Wu R C, Wang G X (2013). On the Ordovician, Silurian boundary with strata in southwestern Hubei, and the Yichang Uplift. Journal of Stratigraphy, 37(3): 265–274

Wang Z C, Zhao W Z, Peng H Y (2002). Characteristics of multi-source petroleum systems in Sichuan basin. Petroleum exploration and development, 29(2): 26–28 (in Chinese)

Wu J S, Yu B S, Li Y X (2012). Adsorption Capacity of Shale Gas and Controlling Factors from the Well Yuye 1 at the Southeast of Chongqing. Journal of Southwest Petroleum University: Science and Technology Edition, 34(4): 40–48 (in Chinese)

Xiao Z H, Yang R F, Feng T, Cao Y J, Wang Q R, Yang T C, Wang C H, Deng Y (2012). Reservoir forming conditions and exploration potential of shale gas in Lower Cambrian Niutitang Formation,

Northwestern Hunan. Journal of Hunan University of Science and Technology(Natural Science Edition), 36(2): 65–70

Xie X M, Teng G R, Qin J Z, Bian L Z, Zhang Q Z, Zhang W T (2013). Bacter-like fossil in the early Cambrian siliceous shale from Zunyi, Guizhou, SW China. Acta Geol Sin, 87(1): 20–28

Zhang T W, Ellis G S, Ruppel S C, Milliken K, Yang R S (2012). Effect of organic-matter type and thermal maturity on methane adsorption in shale-gas systems. Org Geochem, 47: 120–131

Zhou S W, Jiang W, Zhang C Y (2012). The enlightenment on shale gas exploration and development in China getting from Eagle Ford in America. Eng Sci, 14(6): 16–21

Zou C N, Yang Z, Zhang G S, Hou L H, Zhu R K, Tao S Z, Yuan X, Dong , Wang Y, GuoQ , Wang L, Bi H, Li D, WuN (2014). Conventional and unconventional petroleum "orderly accumulation": Concept and practical significance. Petroleum Exploration and Development, 41(1): 14–30